Acta Cryst B
STRUCTURAL SCIENCE
CRYSTAL ENGINEERING
MATERIALS

ISSN 2052-5206

Distorted Te nets in the modulated crystal structures of $RE\mathrm{Te}_{1.94(1)}$ (RE = La, Pr, Nd)

Hagen Poddig and Thomas Doert*

Faculty of Chemistry and Food Chemistry, Technische Universität Dresden, Bergstraße 66, Dresden, 01069, Germany. *Correspondence e-mail: thomas.doert@tu-dresden.de

Received 29 June 2020
Accepted 14 October 2020

Edited by M. Dusek, Academy of Sciences of the Czech Republic, Czech Republic

Dedicated to Professor Sven Lidin on the occasion of his 60th birthday.

Keywords: rare earth metal tellurides; modulated crystal structures; polychalcogenides.

B-IncStrDB reference: 16592EwKlsV

CCDC references: 2012376; 2012379; 2012380

Supporting information: this article has supporting information at journals.iucr.org/b

The two-dimensionally incommensurately modulated crystal structures of the compounds $RE\mathrm{Te}_{1.94\,(1)}$ (RE = La, Pr, Nd) were investigated by single-crystal X-ray diffraction. The compounds crystallize in the tetragonal superspace group $P4/n(\alpha\beta\frac{1}{2})00(-\beta\alpha\frac{1}{2})00$ (No. 85.2.58.2) with $q_1 = \alpha a^* + \beta b^* + \frac{1}{2}c^*$ and $q_2 = -\beta a^* + \alpha b^* + \frac{1}{2}c^*$ and share a common motif of an alternating stacking of a puckered [RETe] layer and a planar [Te] layer. This basic structural motif is observed for all reported compounds with unusually large anisotropic displacement parameters in the planar [Te] layer. Taking the modulation into account, a distortion from this perfect square planar net is noted along with vacancies in the planar [Te] layer. The distortion leads to the formation of different discrete anions, like Te^{2-}, Te_2^{2-} and Te_3^{2-}, similar to previously reported structures for $REX_{2-\delta}$ compounds (RE = trivalent rare earth metal, X = S, Se, Te). The Te–Te distances in the modulated [Te] layer are found in a narrow range as compared to those in the corresponding sulfides and selenides.

1. Introduction

The crystal structures observed for the rare earth metal polychalcogenides $REX_{2-\delta}$ (RE = Y, La–Nd, Sm, Gd–Lu; X = S, Se, Te; $0 \leq \delta \leq 0.2$) show a broad variety of different patterns, including conventional commensurate and incommensurately modulated superstructures based on a common basic unit cell. The basic unit cell features an alternating stacking of a [REX] layer and a [X] layer. This kind of motif is shared by a variety of matlockite-related structures (Nuss & Jansen, 2002; Nuss *et al.*, 2006), where the ZrSSi structure is usually referred to as the common aristotype for the $REX_{2-\delta}$ compounds. The ZrSSi structure features a puckered [ZrS] double layer, which is sandwiched by square planar layers of [Si]. The structure of the REX_2 compounds adopts the same puckered [REX] layer with a slightly different planar chalcogenide layer. As only trivalent RE^{3+} cations and divalent X^{2-} anions are assumed to be present in the puckered layer, the chalcogen atoms of the planar layers carry a formal charge of −1 which leads to a distortion from the ideal square net by forming different polychalcogenide anions, most prominently X_2^{2-} anions.

The phase width δ of the $REX_{2-\delta}$ compounds adds another parameter to the distortion in the planar [X] layer by introducing vacancies and forcing the layer to compensate the charge of the missing X atoms. This is usually achieved by forming a more or less isolated X^{2-} anion for every vacancy along the X_2^{2-} anions, resulting in an average charge of $[X]_{1-\delta}^{-}$, as described for the $CeSe_{1.9}$-type and the $Gd_8Se_{15-\delta}$-type structures (Doert & Müller, 2016). However,

in contrast to the sulfides and selenides, where this rule of thumb is satisfied for all structures, a different scenario has been observed for the tellurides with a composition of $RE\mathrm{Te}_{1.8}$ (RE = Sm, Gd–Dy) (Ijjaali & Ibers, 2006; Poddig *et al.*, 2018). Here, a larger polyanionic telluride fragment, an XeF_2 analogous Te_3^{4-} anion, compensates for a less dense [Te] layer (Poddig *et al.*, 2018). Motivated by this unique situation, structure investigations of further deficient rare earth metal tellurides seem promising.

Aside from conventional commensurate superstructures of the basic ZrSSi unit cell, like $CeSe_{1.9}$- or $GdTe_{1.8}$-type structures, several incommensurately modulated structures have been reported, *e.g.* $GdS_{1.82}$ (Tamazyan *et al.*, 2003), $RE\mathrm{Se}_{1.84\,(1)}$ (RE = La–Nd, Sm) (Graf & Doert, 2009; Doert *et al.*, 2007), or $DySe_{1.84}$ (van der Lee *et al.*, 1997). Interestingly, most of the listed compounds are described in superspace group $P4/n(\alpha\beta\frac{1}{2})00(-\beta\alpha\frac{1}{2})00$ (No. 85.2.58.2), though with different values for α and β, resulting in their unique structural features. These structures show a similar pattern of X^{2-} and X_2^{2-} anions along with some vacancies as observed for the commensurate superstructures of the sulfides and selenides. However, one recent report for $LaTe_{1.82\,(1)}$ describes an incommensurately modulated superstructure for the tellurides, featuring larger polyanionic Te_m^{n-} fragments along with isolated Te^{2-} and Te_2^{2-} anions (Poddig *et al.*, 2020). The existence of incommensurately modulated structures for the tellurides is not surprising, when looking at the related $RE\mathrm{Te}_3$ compounds, which feature an additional planar [Te] layer. The structure observed for these compounds show a one-dimensional modulation, affecting the bonding situation in the planar [Te] layers. Here, mostly V-shaped Te 'trimers' and N-shaped 'tetramers' have been observed along with isolated Te^{2-} anions (Malliakas *et al.*, 2005). Similar results were also reported for mixed $RE\mathrm{SeTe}_2$ (La–Nd, Sm) compounds, which again show a distortion from a perfect square [Te] net (Fokwa Tsinde & Doert, 2005).

These hints from literature gave reason to investigate some further Te-deficient compounds $RE\mathrm{Te}_{2-\delta}$ compounds in detail. We report in the following on the Te-deficient compounds of the composition $RE\mathrm{Te}_{1.94\,(1)}$ (RE = La, Pr, Nd), which highlights a significant difference to the corresponding sulfide and selenide systems where this composition is not documented.

2. Experimental

2.1. Synthesis

All preparation steps were carried out in an argon (purity of 5.0; Praxair Deutschland GmbH, Düsseldorf, Germany) filled glovebox (MBraun, Garching, Germany). Crystals were grown by flux reaction in an alkali halide flux. In a standard synthesis, 500 mg of a stoichiometric mixture of the rare earth metal (RE: 99.5%, MaTecK) and tellurium (Merck, > 99.9%, reduced in H_2 stream at 400°C) was thoroughly mixed with KI (1.5 g, AppliChem, p.a., dried at 200°C under vacuum prior to use) before placing the mixture in a glassy carbon crucible inside a quartz ampoule. The quartz container was flame sealed under dynamic vacuum ($p \leq 1 \times 10^{-3}$ mbar) and the sample was heated with a ramp of 2 K min^{-1} to 1073 K and kept at this temperature for seven days. After this time, the ampoule was slowly cooled with a rate of 0.5 K min^{-1} to 673 K, followed by quick cooling to room temperature. The product was washed with deionized water to remove the alkali halide flux, before washing with ethanol and drying under vacuum. The obtained black crystals can be handled under atmospheric conditions, although we observed a slow degrading of the compounds. Therefore, the samples were stored under an argon atmosphere and the experiments were prepared and realized under atmospheric conditions.

A second approach to synthesize the rare earth metal tellurides is utilizing I_2 in a chemical transport reaction. In a standard synthesis, 500 mg of a stoichiometric mixture of the rare earth metal and tellurium were placed in a quartz tube and flame sealed under dynamic vacuum ($p \leq 1 \times 10^{-3}$ mbar). The ampoule was slowly heated with a ramp of 2 K min^{-1} to 1173 K. The transport takes place in a gradient from 1173 K to 1073 K with I_2 (Roth, > 99.8%, purified by sublimating twice prior to use) as transporting agent. After seven days, the ampoule was cooled to room temperature.

2.2. Single crystal

Single crystal X-ray diffraction was performed with the two-circle diffractometer IPDS II (STOE & Cie, Darmstadt, Germany) equipped with an image plate detector using graphite-monochromated Mo $K\alpha$ radiation (λ = 0.71073 Å) at 296 (1) K. The software package *X-Area* (STOE & Cie, 2009) was used for data collecting, determination and refinement of the lattice parameters as wells as the modulation wavevector components, data integration and correction for Lorentz and polarization factors. A numerical absorption correction based on refined crystal shapes has been performed again with the *X-Area* software package for the average structures, whereas the data of the (3+2)D modulated crystal structure has been corrected with the routine implemented in *Jana2006* (Petříček *et al.*, 2014). The average structures were solved using the dual space approach of the program package *SHELXT* (Sheldrick, 2015*b*). Structure refinement was performed with the program package *SHELXL* against F^2 including anisotropic displacement parameters for all atoms (Sheldrick, 2015*a*). The average crystal structures of the data sets of the (3+2)D modulated crystal structures were solved using the charge-flipping method of the program *Superflip* (Palatinus & Chapuis, 2007) implemented in the *Jana2006* software and the subsequent refinement has been performed with the *Jana2006* software (Petříček *et al.*, 2014). Structure refinement was performed against F^2 including anisotropic displacement parameters for all atoms. Second-order satellites were neglected because of their low intensity (about 99% of these reflections were found with intensities below $3I/\sigma$) and two harmonic waves have been used for the fit of the atomic modulation functions. The two different domains were integrated and corrected independently, as the absorption correction of a (3+2)D hklf5 file was unsatisfactory. The second domain was added to the

Table 1
EDS results (normalized to the *RE* content) on selected single crystals.

Compound	*RE*	Te
La	1.00 (1)	1.94 (1)
Pr	1.00 (4)	1.91 (4)
Nd	1.00 (1)	1.92 (1)

refinement in *Jana2006* as a separate reflection file. Structure images were created with *DIAMOND* (Brandenburg, 2019). Further details on the crystal structure investigations can be obtained from the Fachinformationszentrum Karlsruhe, 76344 Eggenstein-Leopoldshafen, Germany (fax: (+49)7247-808-666; e-mail: crysdata@fiz-karlsruhe.de), on quoting the depository numbers 2012376 ($LaTe_{1.94(1)}$), 2012379 ($NdTe_{1.93(1)}$), 2012380 ($PrTe_{1.94(1)}$).

2.3. Scanning electron microscopy and EDS

Scanning electron microscopy (SEM) was performed with a Hitachi SU8020 microscope with a triple detector system for secondary and low-energy backscattered electrons (U_a = 5 kV). The composition of selected single crystals was determined by semi-quantitative energy-dispersive X-ray analysis (U_a = 20 kV) with a silicon drift detector (SDD) X-Max^N (Oxford).

2.4. Temperature-dependent electrical resistance

The electrical resistance of $LaTe_{1.94(1)}$ was measured between 2.5 and 360 K with a mini-CFMS (Cryogenic Ltd, London). Four gold contacts were attached to the surface of a single crystal in a linear set-up with a silver conductive composite ACHESON 1415 (Plano GmbH) to establish the electrical contact between the crystal and the gold wires.

3. Results and discussion

Black, plate-like single crystals of $LaTe_{1.94(1)}$, $PrTe_{1.94(1)}$ and $NdTe_{1.93(1)}$ were obtained by either alkali halide flux reactions or mineralization with I_2 as transporting agent and showed different advantages. The mineralization experiments yielded larger crystals compared to alkali halide flux reactions, which proved to be useful to grow crystals for a physical characterization. The crystals grown by molten alkali halide flux, on the other hand, were better suited for single-crystal diffraction experiments, as less intergrowth of several individuals has been observed. Side phases, *e.g.* compounds with a lower Te content like $NdTe_{1.89(1)}$, can be avoided by controlling the ratio of the rare earth metal and tellurium. Special care has to be taken when performing the mineralization experiments, as the Te-richer $RETe_3$ compounds can be formed if the initial ratio of the rare earth metal and tellurium is not corrected for the amount of REI_3 formed due to the addition of I_2 (Poddig *et al.*, 2018). Powder and single-crystal diffraction clearly indicate a tetragonal basic unit cell for all compounds with $a \simeq 4.4$ Å and $c \simeq 9.1$ Å, as also seen for $LaTe_{1.82(1)}$ (Poddig *et al.*, 2020). The EDS analysis of different single crystals, give a ratio *RE*:Te of about 1:1.9 (Table 1), which was later on confirmed by the structure refinements.

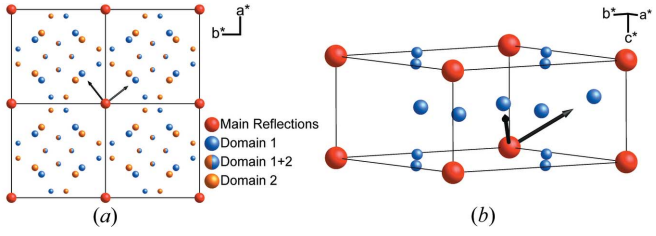

(*a*) (*b*)

Figure 1
(*a*) Projection of the relative positions of the first-order (medium spheres in blue and gold) and second-order satellites (small spheres) with respect to the main reflections (large red spheres) along the [001] direction. (*b* Distribution of the satellites of domain 1 indicating the translational part along **c***.

Table 2
Relative position of the superstructure reflections with respect to the main reflections.

Compound	α	β	γ
$LaTe_{1.94(1)}$	0.249 (1)	0.330 (1)	$\frac{1}{2}$
$PrTe_{1.94(1)}$	0.253 (1)	0.323 (1)	$\frac{1}{2}$
$NdTe_{1.93(1)}$	0.263 (1)	0.329 (1)	$\frac{1}{2}$

Single crystal diffraction at ambient temperature revealed additional weak reflections in the *hkn* (n = 0, 1, 2 . . .) layer and slightly stronger reflections in the *hkn* ($n = \pm 0.5, \pm 1.5 \ldots$) layer, with respect to the basic tetragonal unit cell. A similar situation has been observed for the recently reported compound $LaTe_{1.82(1)}$, where additional reflections are noted in the *hkn* (n = ±0.5, ±1.5 . . .) layers. However, unlike for $LaTe_{1.82(1)}$, eight strong satellite reflections, alongside several weak reflections, are essentially present around one main reflection in the *hkn*.5 layers of the title compounds (Fig. S1). Only half of the satellite reflections can be described with two q vectors, *i.e.* by a two-dimensional modulation, for the description of all other reflections an additional twinning phenomenon needs to be taken into account (Fig. 1). Considering two merohedral twin domains with Laue symmetry 4/*m* yields a fully indexable diffraction pattern, making an intergrowth compound unlikely (van Smaalen & Petříček, 1992). The symmetry reduction is necessary, as the modulation wavevector components α and β are different and, thus, not compatible with 4/*mmm* Laue symmetry but match the conditions for the Laue class 4/*m*. The modulated $RESe_{1.84(1)}$ (*RE* = La–Nd, Sm) compounds showed a similar twinning, although a comparable clear differentiation between the two domains from the diffraction images has not been reported (Graf & Doert, 2009; Doert *et al.*, 2007).

Using the superspace approach, the modulation wavevectors q_1 and q_2 for indexing of the diffraction patterns of the compounds $RETe_{1.94(1)}$ (*RE* = La, Pr, Nd) are $q_1 = \alpha a^* + \beta b^* + \frac{1}{2}c^*$ and $q_2 = -\beta a^* + \alpha b^* + \frac{1}{2}c^*$ with components α, β and γ given in Table 2, describing the [3+2] dimensional incommensurately modulated structures.

The weak reflections in the *hkn* (n = 0, ±1, ±2 . . .) layers can be explained by the linear combination of q_1 and q_2, which

Table 3
Unit-cell parameters, Te2 occupation and refinement indicators of the $RE\mathrm{Te}_{1.94\,(1)}$ average structures.

	a (Å)	c (Å)	occ. (Te2)	R_1/wR_2
La	4.5226 (6)	9.147 (1)	0.932 (5)	0.0189/ 0.0433
Pr	4.4535 (5)	9.047 (1)	0.943 (6)	0.0292/ 0.0564
Nd	4.4274 (6)	9.029 (1)	0.923 (6)	0.0237/ 0.0420

supports our assumption of a [3+2] dimensional superstructure (Fig. S1). As mentioned above, the observed satellite reflections are compatible with a fourfold rotational axis, which is shown in an idealized, schematic diffraction image in Fig. 1. In contrast to the similarly twinned modulated rare earth metal selenides $RE\mathrm{Se}_{1.84\,(1)}$ (RE = La–Nd, Sm) with nearly identical modulation wavevector components $\alpha \simeq \beta \simeq 0.293$ (1) (Doert *et al.*, 2007; Graf & Doert, 2009), α and β are clearly distinguishable in the case of the tellurides $RE\mathrm{Te}_{1.94\,(1)}$ (RE = La, Pr, Nd), resulting in two separate and distinguishable sets of satellite reflections.

3.1. Average crystal structure

As the diffraction patterns and, hence, the modulated structures of the three title compounds are very similar, the discussion of the structural data will be outlined on $\mathrm{LaTe}_{1.94\,(1)}$ in detail. The main reflections of all compounds can be indexed with a basic tetragonal unit cell and the dimensions of the unit-cell parameters deviate slightly for each rare earth element as shown in Table 3. Structure solution and refinements have been performed in space group *P*4/*nmm* (No. 129) in accordance with the space group of the ZrSSi aristotype. Note that the general reflection condition observed (reflections *hk*0 only present if $h + k = 2n$) is also compatible with *P*4/*n* (No. 85), which is a t2 subgroup of *P*4/*nmm*. The refined average structure shows an alternating stacking of a puckered [LaTe] layer and a square planar [Te] layer. EDS results point towards a ratio La:Te of about 1:1.9 (Table 1), indicating a reduced site occupancy on one Te site. In accordance with previous results on other commensurate superstructures as *e.g.* $\mathrm{CeTe}_{1.9}$ (Ijjaali & Ibers, 2006) and incommensurately modulated structures such as *e.g.* $\mathrm{LaTe}_{1.82\,(1)}$ (Poddig *et al.*, 2020) a reduced site occupancy should only be present in the planar Te layer. Hence, a freely refined site occupancy factor of Te2 converged with about 0.93 (1) as expected.

The average structure of $\mathrm{LaTe}_{1.94\,(1)}$ is displayed in Fig. 2. Compared to the previously reported structure of $\mathrm{LaTe}_{1.82\,(1)}$ (Poddig *et al.*, 2020) and the compounds of the series $RE\mathrm{Se}_{1.84\,(1)}$ (RE = La–Nd, Sm) (Graf & Doert, 2009; Doert *et al.*, 2007), the anisotropy of the atomic displacement parameters (ADPs) is less pronounced for the respective atoms of the title compounds, but hint towards similar effects of the modulation in the crystal structures. The elongated ADPs in the *ab* plane of Te2 point towards a displacement of Te inside the [Te] layer, forming different (poly)anions. The reduced site occupancy factor is a result of vacancies in the planar [Te] layer of the modulated structure. The average structure of $\mathrm{LaTe}_{1.94\,(1)}$ shows a Te–Te distance of 3.1980 (4) Å, which is larger than the usual observed bond length for a $\mathrm{Te_2}^{2-}$ anion with about 2.80 Å (Böttcher *et al.*, 1993). However, larger Te–Te distances are expected for the average structure, as similar distances of 3.1821 (4) Å have been observed for $\mathrm{LaTe}_{1.82\,(1)}$ (Poddig *et al.*, 2020). The ADPs of La1 and Te1 are only slightly elongated along the [001] direction, most probably as a reaction of the metal cation to the modulation in the [Te] layer. Due to the small amount of vacancies, this tendency is less pronounced as compared to $\mathrm{LaTe}_{1.82\,(1)}$ or the $RE\mathrm{Se}_{1.84\,(1)}$ (RE = La–Nd, Sm) compounds. The coordination polyhedron around the La atom only is a nearly undistorted capped square antiprism formed by five Te atoms from the [LaTe] layers with distances of 4 × 3.3121 (5) Å and 1 × 3.303 (1) Å, and by four additional Te atoms from the planar layer with distances of 3.3643 (6) Å.

3.2. Modulated crystal structure

The development of a structural model was performed analogous to the procedure for $\mathrm{LaTe}_{1.82\,(1)}$ reported recently (Poddig *et al.*, 2020) by considering first group-subgroup relations starting from the highest possible three-dimensional space group *P*4/*nmm* (No. 129). The components of the two different q vectors do not meet the conditions of a superspace group in the high Laue class 4/*mmm* and enforce a symmetry reduction to 4/*m* or lower symmetry. A similar symmetry reduction has been reported for $RE\mathrm{Se}_{1.84\,(1)}$ (RE = La–Nd, Sm) (Graf & Doert, 2009; Doert *et al.*, 2007), resulting in space group *P*4/*n* (No. 85) for the basic structure. In contrast to the reported selenides, the c axis has not been doubled for the tellurides to meet the conditions of an *X*-centred unit cell, where the main reflections in the *hkn*.5 layer are treated as systematically absent. Considering the modulation wavevec-

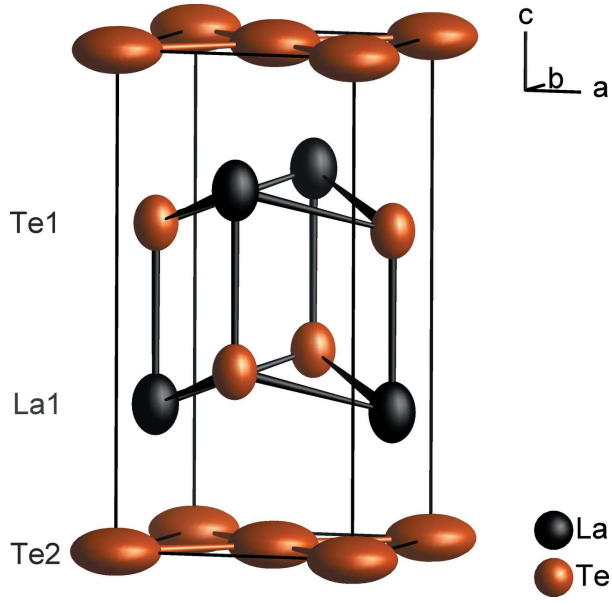

Figure 2
Average structure of $\mathrm{LaTe}_{1.94\,(1)}$ refined in *P*4/*nmm*. Ellipsoids are drawn with a probability of 99.9%.

Table 4
Crystallographic data and refinement details on the compounds $RE\mathrm{Te}_{1.94\,(1)}$.

For all structures: space group $P4/n(\alpha\beta\frac{1}{2})00(-\beta\alpha\frac{1}{2})00$ (No. 85.2.58.2), modulation wavevectors $q_1 = \alpha a^* + \beta b^* + \frac{1}{2}c^*$, $q_2 = -\beta a^* + \alpha b^* + \frac{1}{2}c^*$, $Z = 2$. All experiments carried out at 296 (1) K on a STOE IPDS II diffractometer with Mo $K\alpha$ radiation ($\lambda = 0.71073$ Å).

	$LaTe_{1.94\,(1)}$			$PrTe_{1.94\,(1)}$			$NdTe_{1.93\,(1)}$		
Reference composition	$LaTe_{1.944\,(3)}$			$PrTe_{1.944\,(2)}$			$NdTe_{1.927\,(3)}$		
Formula weight (g mol^{-1})	387.0			389.09			390.1		
$F(000)$	316			320			320		
Crystal size (mm)	0.18 × 0.06 × 0.05			0.10 × 0.05 × 0.02			0.34 × 0.09 × 0.01		
Unit-cell parameters (Å)	$a = 4.5226\,(6)$, $c = 9.145\,(1)$			$a = 4.4508\,(4)$, $c = 9.0490\,(8)$			$a = 4.4278\,(6)$, $c = 9.026\,(1)$		
Index range measured	$-6 \le h \le 6$; $-6 \le k \le 6$; $-13 \le l \le 13$; $-1 \le m, n \le 1$			$-6 \le h \le 6$; $-6 \le k \le 6$; $-13 \le l \le 13$; $-1 \le m, n \le 1$			$-6 \le h \le 6$; $-6 \le k \le 6$; $-13 \le l \le 13$; $-1 \le m, n \le 1$		
θ_{min}, θ_{max}, (°)	2.17, 31.82			2.20, 29.32			2.25, 29.33		
No. of measured reflections	21 190			39 908			33 812		
μ (mm^{-1})	26.415			29.085			30.452		
T_{min}, T_{max}	0.0616, 0.2286			0.0241, 0.4601			0.0242, 0.6807		
Extinction parameter (Becker & Coppens, 1974)	0.053 (3)			0.330 (7)			0.402 (1)		
No. of independent reflections	2260, 997 > $3\sigma(I)$			2180, 1087 > $3\sigma(I)$			2161, 876 > $3\sigma(I)$		
No. of main reflections	260, 254 > $3\sigma(I)$			247, 246 > $3\sigma(I)$			245, 242 > $3\sigma(I)$		
No. of first-order satellites	2000, 743 > $3\sigma(I)$			1933, 841 > $3\sigma(I)$			1916, 632 > $3\sigma(I)$		
R_{int}	0.0558, 0.0484 [$I > 3\sigma(I)$]			0.0512, 0.0469 [$I > 3\sigma(I)$]			0.0875, 0.0742 [$I > 3\sigma(I)$]		
R_σ	0.0406, 0.0099 [$I > 3\sigma(I)$]			0.0257, 0.0073 [$I > 3\sigma(I)$]			0.0394, 0.0087 [$I > 3\sigma(I)$]		
Refinement program	*Jana2006*, full matrix against F^2								
No. of restrictions, parameters	0, 40			0, 40			0, 34†		
Twin volume (%)	44.1 (3)			49.1 (2)			41.8 (3)		
Reflections	All	Main	First-order satellite	All	Main	First-order satellite	All	Main	First-order satellite
R_1 [$3\sigma(I)$]	0.0494	0.0233	0.0989	0.0274	0.0186	0.0442	0.0385	0.0251	0.0695
R_1 (all)	0.0992	0.0235	0.1922	0.0509	0.0187	0.0951	0.0718	0.0256	0.1387
wR_2 [$3\sigma(I)$]	0.0909	0.0608	0.1662	0.0718	0.0634	0.0945	0.0949	0.0671	0.1682
wR_2 (all)	0.1017	0.0609	0.1949	0.0738	0.0635	0.1005	0.0972	0.0671	0.1739
Goof [$3\sigma(I)$/all]	2.19, 1.61			1.81, 1.30			2.42, 1.56		
Largest diff. peak, hole (e Å^{-3})	5.31, −4.24			2.90, −2.82			5.06, −4.83		

† Due to large correlations, the modulation parameters of the ADPs of Te2 were refined considering one twin domain first and fixed to these values in the final least-squares cycles considering both domains.

tors and their components (see above) results in the superspace group $P4/n(\alpha\beta\frac{1}{2})00(-\beta\alpha\frac{1}{2})00$ (No. 85.2.58.2) (Stokes *et al.*, 2011). As pointed out in the discussion of the diffraction image, twinning was taken into account, which is likely due to the t2 symmetry reduction. The twin law (010 100 00$\bar{1}$) has been introduced for all three structures, converging to a twin volume of about 44% for $LaTe_{1.94\,(1)}$.

The atomic modulation functions (AMF) have been added stepwise to the refinement. The positional displacement of all atoms has been modelled first, before introducing the occupational modulation function for the Te2 atoms and finally adding modulation functions to the ADPs. For all parameters, two harmonic modulation functions were used. Introducing AMFs for the ADPs was especially crucial for modelling the Te2 atom in the [Te] layer to compensate for overshooting and truncation effects, which greatly reduced the residual electron density. Details on the refinement are given in Table 4.

The displacements of all atoms along *a*, *b* and *c* are displayed in Fig. 3 [see Fig. S4 for $PrTe_{1.94\,(1)}$ and $NdTe_{1.93\,(1)}$]. The most pronounced displacement in the [LaTe] layer is seen along the [001] direction, as already hinted at by the average structure. Additionally, this plot emphasizes the larger influence of the modulation on La1 as compared to Te1, which can best be seen along the *c* direction, where Te1 follows the movement of La1, however, with a smaller displacement. The different amounts of the displacements can also be seen in the corresponding F_{obs} plots in Figs. S2 and S3, respectively. From a crystal-chemically point of view, this is not surprising, as La1 tries to maintain its coordination sphere which is partly fragmented by vacancies in the planar [Te] layer and the respective re-arrangement of the telluride anions. This is achieved by getting closer to the [Te] layer, which in return forces the Te1 atom to react to the displacement of La1. A different situation is observed for Te2 in the [Te] layer, where only a displacement in the *ab* plane is observed and the displacement along the [001] direction is negligible. Moreover, the comparison of the displacements with $LaTe_{1.82\,(1)}$ shows another interesting feature. The total displacement for $LaTe_{1.94\,(1)}$, as shown in Figs. 3(*a*) and 3(*b*), is considerably smaller (roughly by a factor of two) than in $LaTe_{1.82\,(1)}$. This can mainly be attributed to the higher Te content in the [Te] layer of the $RE\mathrm{Te}_{1.94\,(1)}$ compounds, resulting in less void space for their displacements, but also a reduced need for structural reorganization. For a fully occupied [Te] layer in $LaTe_2$, a double-herringbone pattern of dinuclear Te_2^{2-} dianions was reported (Stöwe, 2000*a*) with only small differences between bonding and non-bonding Te···Te distances. Introducing even small amounts of vacancies results in the formation of charge-compensating Te^{2-} anions and, hence, changes the local environment of the remaining Te_2^{2-} anions while maintaining a more or less close packed [Te] layer. As more and more vacancies are introduced, this close packing of dinuclear anions falls apart, allowing for a higher degree of freedom and increases the displacement of the Te2 atoms with respect to the basic ZrSSi-

type structure. Going along with the increasing number of vacancies, different ordering patterns have been found, like the patterns in $CeTe_{1.9}$, crystallizing in the $CeSe_{1.9}$-type (Ijjaali & Ibers, 2006) or $NdTe_{1.89\,(1)}$ crystallizing in the Gd_8Se_{15}-type structure (Stöwe, 2001).

The Te2–Te2 distances observed for $LaTe_{1.94\,(1)}$ range from 2.924 (3) Å to 3.473 (3) Å [Fig. 4(*a*)] with an average distance of 3.206 (2) Å. These distances match the observed distances for $LaTe_2$ quite well, where Te–Te distances between 2.988 (2) Å and 3.406 (2) Å are reported (Stöwe, 2000*a*). As mentioned in the discussion of the average structure, these distances are quite large compared to isolated Te_2^{2-} anions, *e.g.* (Böttcher *et al.*, 1993), although very common for the stoichiometric rare earth metal tellurides $LaTe_2$, $CeTe_2$ and $PrTe_2$ (Stöwe, 2000*a*,*b*,*c*).

The investigation of the different *t*-plots of Te2 showed two extreme values of *u*, respectively *x*5, at 0 and 0.5, which is best visualized in the F_{obs} maps for Te2 (Fig. 5). At u = 0.5 the lowest electron density is observed, consistent with the lowest occupation probability of Te2. However, in contrast to the selenides $RESe_{1.84\,(1)}$ and $LaTe_{1.82\,(1)}$, a real gap indicating zero occupation between two maxima in the F_{obs} plots is not observed for any *t* and *u* or respectively *x*4 and *x*5. This, on the one hand reflects the higher chalcogen content of this compound but may also indicate an underlying, unresolved atomic disorder.

Using a cut-off value of about 0.825 for the occupation of the Te2 position as indicated in Fig. 4(*b*) and used in the F_{obs} maps (Fig. 5), the Te2–Te2 distance plot [Fig. 4(*a*), see Figs. S5 for $PrTe_{1.94\,(1)}$ and $NdTe_{1.93\,(1)}$] allows for an interpretation as isolated Te^{2-} anions. For u = 0.5, the largest Te2–Te2 distances can be observed with distances ranging from about 3.003 Å to 3.473 Å [Fig. 4(*a*)], which could be interpreted as a region containing mainly isolated Te^{2-} anions. In the interval from $0.5 \leq u \leq 0.65$, the observed distances spread again, indicating shorter, bonding interactions and larger, non-bonding interactions for the different Te2 atoms [Fig. 4(*a*)]. Looking at the plot of the occupancy of Te2 against *t* reveals, that this is mainly a consequence of the rising Te content in the planar [Te] layer, forcing the Te atoms to get closer to each other.

3.3. Discussion of the modulated crystal structure of $LaTe_{1.94\,(1)}$

A representative section of the modulated crystal structure of $LaTe_{1.94\,(1)}$ is displayed in Fig. 6 and Fig. S6. The general features of the average structure are maintained, like the alternating stacking of a puckered [LaTe] layer and a planar [Te] layer. As expected from the discussion of the *t*-plots, a small movement of the puckered [LaTe] layer towards the planar [Te] layer is observed. The more interesting changes introduced by the modulation can be seen in the planar [Te] layer.

The planar [Te] layer features mainly Te_2^{2-} dumbbells and isolated Te^{2-} anions along with some vacancies and bent Te_3 units. Allowing higher occupancy cut-off values than 0.825 additionally result in apparent Te_4 squares with Te–Te distances of about 2.93 (1) Å, which have also been discussed

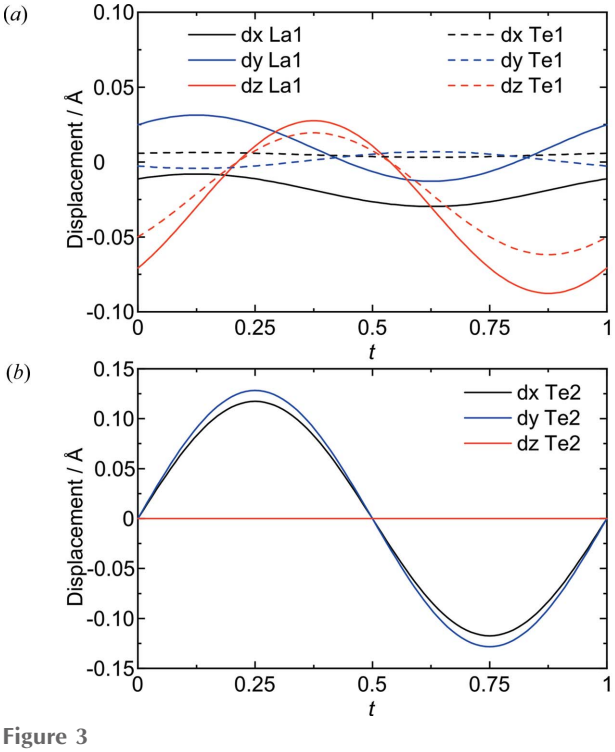

Figure 3
t-plot of the displacements of La1 and Te1 in the [LaTe] layer (*a*) and of Te2 in the [Te] layer (*b*).

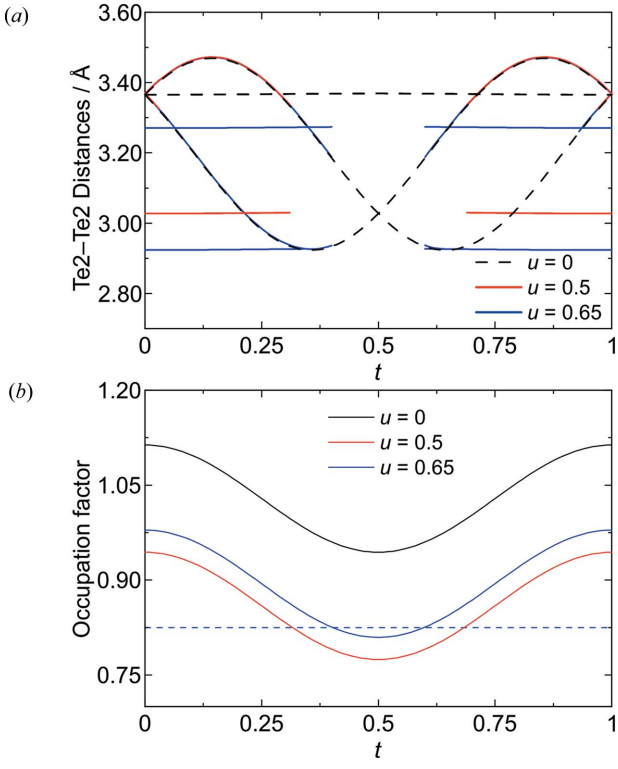

Figure 4
t-plots of the Te2–Te2 distances with a cut-off value of 0.825 (*a*) and the site occupation factor of Te2 (*b*); the blue dashed line in (*b*) indicates the average occupation factor.

for different $RE\mathrm{Te}_{2-\delta}$ compounds, like CeTe_2, PrTe_2 and $\mathrm{LaTe}_{1.82\,(1)}$ (Stöwe, 2000*b*,*c*; Poddig *et al.*, 2020). However, these Te_4 fragments are presumably the result of an unresolved disorder of two differently orientated Te_2^{2-} anions and two adjacent vacancies in the [Te] layer.

The observed bent Te_3 fragments are part of a larger Te_8 ring, emphasized in Fig. S6, as already reported for $\mathrm{NdTe}_{1.89\,(1)}$ (Stöwe, 2001) and $\mathrm{LaTe}_{1.82\,(1)}$. The ordering pattern of a Te_8 ring around a vacancy by four Te_2^{2-} anions with alternating short and long distances is additionally observed. The latter resembles the pattern of the $\mathrm{CeSe}_{1.9}$ structures very well. Because the title compounds are compositionally intermediate between the stoichiometric ditellurides $RE\mathrm{Te}_2$ and the $RE\mathrm{Te}_{1.9}$ phases, their structures may be rationalized as a combination of the double herringbone pattern of Te_2^{2-} anions observed in $RE\mathrm{Te}_2$, and a $\mathrm{CeSe}_{1.9}$-type pattern, which shows a regular ordering of an eight-membered Te ring around a central vacancy plus an isolated Te^{2-} anion. A combination of these motifs is indeed visible in the modulated Te layer, where a double herringbone like distribution of the Te_2^{2-} anions is observed complemented by isolated Te^{2-} anions and a few Te_3^{2-}-shaped anions (Fig. S6). This motif seems to have its origin at an eight-membered Te ring, as displayed in Fig. 6(*b*).

As the reported $RE\mathrm{Te}_{1.9+\delta}$ compounds show a comparably low amount of vacancies, their influence on the shape on the [Te] layer will be discussed with regard to the recently published tellurides and the analogous sulfides and selenides. Vacancy ordering is quite fundamental to these structures, as the chalcogenide layer of the commensurate superstructures of $\mathrm{CeSe}_{1.9}$- and $\mathrm{Gd_8Se_{15}}$-type structures can be rationalized by vacancies, isolated X^{2-} anions and X_2^{2-} dianions (Doert & Müller, 2016). The tellurides show a more ambiguous behaviour compared to the sulfides and selenides, as *e.g.* $\mathrm{GdTe}_{1.8}$-type structures do not fit into this scheme and exhibit a less dense [Te] layer due to a larger polyanionic Te_3^{4-} fragment and no obvious vacancy in the chalcogenide layer (Poddig *et al.*, 2018). The structure of $\mathrm{LaTe}_{1.82\,(1)}$, however, matches partly the motif observed for $\mathrm{Gd_8Se_{15}}$-type structures as vacancies are situated within eight-membered Te rings. Furthermore, larger dumbbell-shaped vacancies dominate the motif in between the Te rings additionally to larger polyanionic fragments. The higher Te content present in $\mathrm{LaTe}_{1.94\,(1)}$ results in considerably fewer vacancies, which are mostly situated inside Te_8 rings, resembling quite well the motif observed for the sulfides and selenides. This observation of very similar structures and vacancy ordering for all three chalcogenides is only noticed for a low vacancy concentration as observed for *e.g.* $\mathrm{CeTe}_{1.9}$ and $\mathrm{NdTe}_{1.89\,(1)}$. Although vacancies are found in a very similar environment for all three chalcogenides, the tellurides still show a distinct tendency to form larger anions, as *e.g.* Te_3^{2-} anions are found in $\mathrm{NdTe}_{1.89\,(1)}$ and $\mathrm{LaTe}_{1.94\,(1)}$.

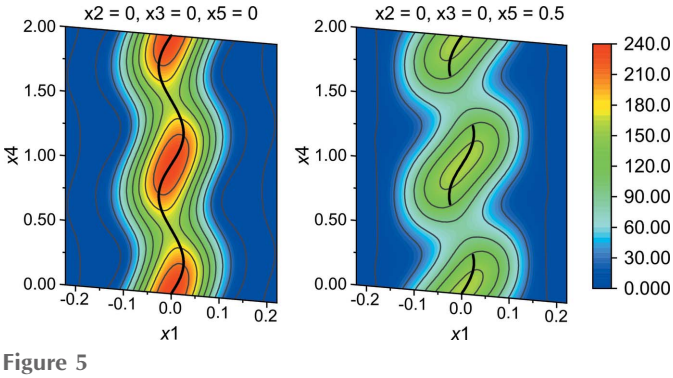

Figure 5
F_{obs} plots of Te2 at $u = 0$ and $u = 0.5$. The solid line indicates the refined AMF for a cut-off value of 0.825. The electron density is displayed in 27.5 e Å^{-3} steps for the contour lines.

3.4. Electrical resistance of $\mathrm{LaTe}_{1.94\,(1)}$

The electrical resistance of $\mathrm{LaTe}_{1.94\,(1)}$ has been measured as a function of the temperature between 2.5 and 360 K by a four-point measurement. As expected from previous reports on these compounds, the electrical resistance increases with decreasing temperature, indicating semiconducting behaviour. Estimating the band gap, E_g, from the recorded data has been done by fitting the high-temperature region according to the Arrhenius-like equation $\rho = \rho_0 \exp(E_g/2k_BT)$, where k_B is the

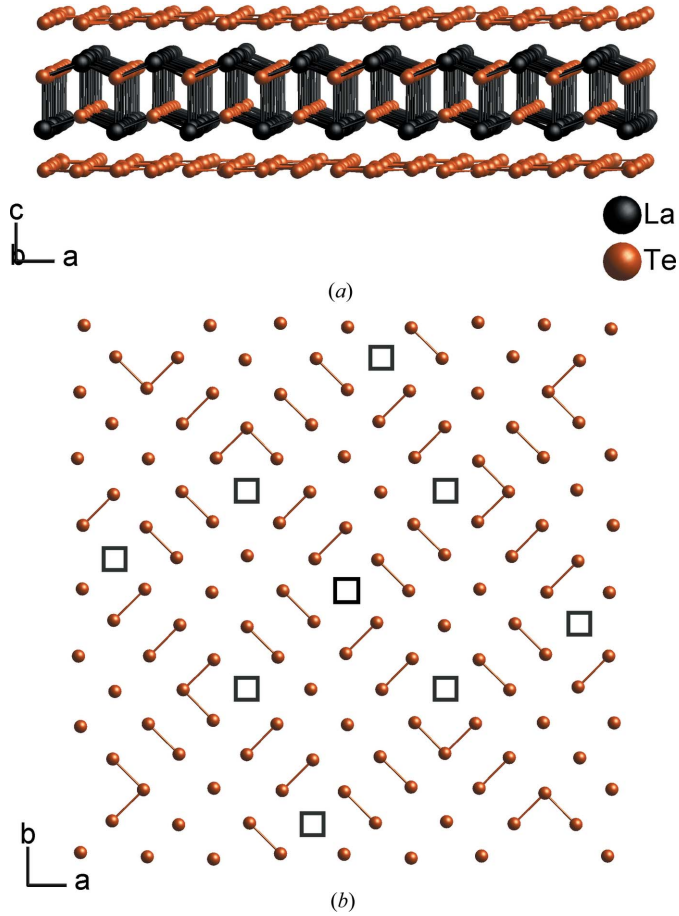

Figure 6
Extended sections of the modulated crystal structure of $\mathrm{LaTe}_{1.94\,(1)}$. The upper panel (*a*) shows the layered motif of an alternating stacking of [LaTe] and [Te] layers. The lower panel (*b*) displays the [Te] layer with an occupation cut-off value set to 0.825. Bonds are drawn between Te atoms in the range 2.926 to 3.012 Å, black squares emphasize vacancies in the [Te] layer.

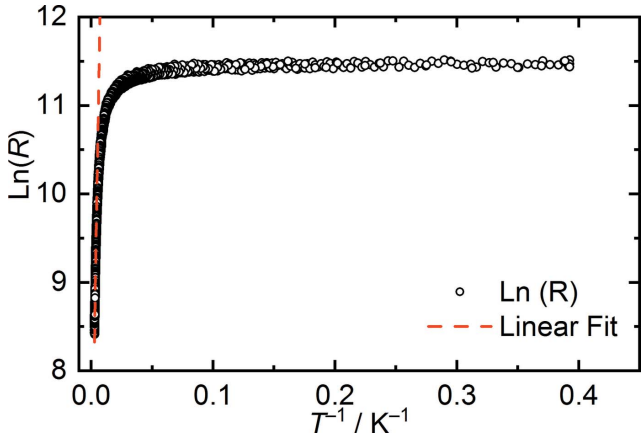

Figure 7
Plot of the logarithmic resistance against the reciprocal temperature between 2.5 and 360 K. The linear fit of the high-temperature region is indicated in red.

Boltzmann constant and T is the absolute temperature. The band gap of $LaTe_{1.94\,(1)}$, according to this fit, is 0.14 eV (Fig. 7), which is similar to the reported band gaps of $NdTe_{1.89\,(1)}$ (0.14 eV) (Stöwe, 2001), $LaTe_{1.82\,(1)}$ (0.17 eV) (Poddig *et al.*, 2020), $GdTe_{1.8}$ (0.19 eV) (Poddig *et al.*, 2018) and $SmTe_{1.84}$ (0.04 eV) (Park *et al.*, 1998). As expected, the band gap of $LaTe_{1.94\,(1)}$ is slightly smaller than the one reported for $LaTe_{1.82\,(1)}$, but matches that of $NdTe_{1.89\,(1)}$ very well, hinting towards a more metallic behaviour with an increasing Te content in the $RETe_{2-\delta}$ series. The only metallic behaviour in this series has been reported for $LaTe_2$ (Stöwe, 2000*a*).

3.5. Conclusion

The modulated crystal structures of the compounds $RETe_{1.94\,(1)}$ (RE = La, Pr, Nd) have been solved and refined in superspace group $P4/n(\alpha\beta\frac{1}{2})00(-\beta\alpha\frac{1}{2})00$ (No. 85.2.58.2) from single crystal data. Unlike the previously reported $LaTe_{1.82\,(1)}$, the tetragonal symmetry is preserved for all compounds. The average crystal structure resembles the structure of the commonly shared aristotype, ZrSSi, with a reduced site occupancy of the Te2 atom to about 94% for $LaTe_{1.94\,(1)}$. Taking the modulation into account, a displacement of both atoms in the [RETe] layer along the [001] direction and, apart from a similar displacive modulation in the *ab* plane, an occupational modulation is observed for the Te2 atoms in the planar [Te] layer. The puckered [RETe] double layer is less affected by the modulation, whereas the modulation leads to vacancies and the formation of different anionic Te fragments in the planar [Te] layer. As expected for a compound of this composition, many similarities with the well known REX_2 and $REX_{1.9}$ structures are observed, like eight-membered Te fragments, isolated Te^{2-} anions along with Te_2^{2-} anions and vacancies. In this sense, the new structures fit well into the series of rare earth metal polychalcogenides $REX_{2-\delta}$.

Acknowledgements

Open access funding enabled and organized by Projekt DEAL.

Funding information

The following funding is acknowledged: Deutsche Forschungsgemeinschaft (grant No. DO 590/6 to Thomas Doert).

References

Becker, P. J. & Coppens, P. (1974). *Acta Cryst.* A**30**, 148–153.
Böttcher, P., Getzschmann, J. & Keller, R. (1993). *Z. Anorg. Allg. Chem.* **619**, 476–488.
Brandenburg, K. (2019). *DIAMOND*, version 4.6.1. Crystal Impact GbR, Bonn, Germany.
Doert, T., Graf, C., Schmidt, P., Vasilieva, I. G., Simon, P. & Carrillo-Cabrera, W. (2007). *J. Solid State Chem.* **180**, 496–509.
Doert, T. & Müller, C. J. (2016). *Binary Polysulfides and Polyselenides of Trivalent Rare-Earth Metals*. In *Reference Module in Chemistry, Molecular Sciences and Chemical Engineering*, edited by J. Reedijk. Elsevier.
Fokwa Tsinde, B. P. & Doert, T. (2005). *Solid State Sci.* **7**, 573–587.
Graf, C. & Doert, T. (2009). *Z. Kristallogr. Cryst. Mater.* **224**, 568–579.
Ijjaali, I. & Ibers, J. A. (2006). *J. Solid State Chem.* **179**, 3456–3460.
Lee, A. van der, Hoistad, L. M., Evain, M., Foran, B. J. & Lee, S. (1997). *Chem. Mater.* **9**, 218–226.
Malliakas, C., Billinge, S. J. L., Kim, H. J. & Kanatzidis, M. G. (2005). *J. Am. Chem. Soc.* **127**, 6510–6511.
Nuss, J. & Jansen, M. (2002). *Z. Anorg. Allg. Chem.* **628**, 1152–1157.
Nuss, J., Wedig, U. & Jansen, M. (2006). *Z. Kristallogr. Cryst. Mater.* **221**, 554–562.
Palatinus, L. & Chapuis, G. (2007). *J. Appl. Cryst.* **40**, 786–790.
Park, S.-M., Park, S.-J. & Kim, S.-J. (1998). *J. Solid State Chem.* **140**, 300–306.
Petříček, V., Dušek, M. & Palatinus, L. (2014). *Z. Kristallogr. Cryst. Mater.* **229**, 345–352.
Poddig, H., Donath, T., Gebauer, P., Finzel, K., Kohout, M., Wu, Y., Schmidt, P. & Doert, T. (2018). *Z. Anorg. Allg. Chem.* **644**, 1886–1896.
Poddig, H., Finzel, K. & Doert, T. (2020). *Acta Cryst.* C**76**, 530–540.
Sheldrick, G. M. (2015*a*). *Acta Cryst.* C**71**, 3–8.
Sheldrick, G. M. (2015*b*). *Acta Cryst.* A**71**, 3–8.
Smaalen, S. van & Petříček, V. (1992). *Acta Cryst.* A**48**, 610–618.
STOE & Cie (2009). *X-AREA*. STOE & Cie GmbH, Darmstadt, Germany.
Stokes, H. T., Campbell, B. J. & van Smaalen, S. (2011). *Acta Cryst.* A**67**, 45–55.
Stöwe, K. (2000*a*). *J. Solid State Chem.* **149**, 155–166.
Stöwe, K. (2000*b*). *J. Alloys Compd.* **307**, 101–110.
Stöwe, K. (2000*c*). *Z. Anorg. Allg. Chem.* **626**, 803–811.
Stöwe, K. (2001). *Z. Kristallogr. Cryst. Mater.* **216**, 215–224.
Tamazyan, R., van Smaalen, S., Vasilyeva, I. G. & Arnold, H. (2003). *Acta Cryst.* B**59**, 709–719.